Available online at www.sciencedirect.com
ScienceDirect
Journal of Power Sources 172 (2007) 246–252
JOURNAL OF POWER SOURCES
www.elsevier.com/locate/jpowsour

Modeling of an anode-supported Ni-YSZ|Ni-ScSZ|ScSZ|LSM-ScSZ multiple layers SOFC cell Part II. Simulations and discussion

Yixiang Shi [a], Ningsheng Cai [a,*], Chen Li [a], Cheng Bao [a], Eric Croiset [b], Jiqin Qian [c], Qiang Hu [c], Shaorong Wang [c]

[a] *Key Laboratory for Thermal Science and Power Engineering of Ministry of Education, Tsinghua University, Beijing 100084, China*
[b] *Department of Chemical Engineering, University of Waterloo, Waterloo, Ontario N2L 3G1, Canada*
[c] *Shanghai Institute of Ceramics, Chinese Academy of Sciences (SICCAS), 1295 Dingxi Road, Shanghai 200050, China*

Received 8 February 2007; received in revised form 19 April 2007; accepted 19 April 2007
Available online 4 May 2007

Abstract

In part I of the present study, a two-dimensional isothermal mechanistic model of a composite yttria/scandia stabilized zirconia anode-supported multiple layers solid oxide fuel cell (Ni-YSZ|Ni-ScSZ|ScSZ|LSM-ScSZ) was developed, calibrated and validated using a button cell setup. In this paper, the model was further validated for extended operating conditions of fuel and oxidant compositions, which confirmed the robustness of the model. Since an important attribute of this model is its ability to accurately describe the effect of cell microstructure on cell performance, a large section of part II is devoted to sensitivity analysis of various microstructure parameters (cathode area, porosity, layer thickness and particle radius) on cell performance. In particular, the simulation results have shown how the button cell microstructure should be modified to optimize its performance. The proposed model could be used as a bridge between micro-scale electrode models and macro-scale unit cell simulation, thus being a useful tool for electrode design.

Keywords: Intermediate temperature solid oxide fuel cell; Anode-supported; Modeling; Electrode microstructure

1. Introduction

In part I of this study, a review of SOFC modeling approaches has been presented [1] and it was shown that high SOFC performance relies on superior electrochemical reactions and mass transport processes. Since experimental studies on SOFC are expensive, time-consuming and labor-intensive, quantitative mechanistic models for the cell PEN (positive electrode|electrolyte|negative electrode) structure are essential for improving SOFC designs. In part I, a two-dimensional isothermal mechanistic model of an anode-supported Ni-YSZ|Ni-ScSZ|ScSZ|LSM-ScSZ multiple layers solid oxide fuel was developed to describe the intricate interdependency among the ionic conduction, electronic conduction, multi-component species transport, electrochemical reaction processes and electrode microstructure. The model is based on the following assumptions: (1) the PEN operates at steady state; (2) all gas mixtures are considered as ideal gases; (3) the reaction active sites are assumed to be uniformly distributed in each electrode layer. The two conducting phases (electronic and ionic) are considered to be continuous and homogeneous in each electrode layer; (4) the temperature is uniform in the PEN, thus the model is assumed isothermal and all physical properties are evaluated at a fixed cell temperature; (5) convection flux is neglected in the porous electrode compared to diffusion. Pressure gradients in the porous electrode are also neglected; (6) the boundary conditions for potential and species concentrations are assumed uniform at the electrode/gas channel interface.

Due to symmetry, a two-dimensional axial symmetrical coordinate is adopted. Refer to Refs. [1,2] for a detailed description of the governing equations. The calculations were

* Corresponding author. Tel.: +86 1062789955; fax: +86 1062789955.
E-mail address: cains@mail.tsinghua.edu.cn (N. Cai).

0378-7753/$ – see front matter © 2007 Elsevier B.V. All rights reserved.
doi:10.1016/j.jpowsour.2007.04.050

performed using the finite element commercial software COMSOL MULTIPHSICS®, Version 3.2.

The model was calibrated and validated by comparing various overpotentials (anodic, cathodic and ohmic) determined experimentally with those determined from simulation.

Beside the development of a comprehensive validated model, another objective of this work was to study the effects of various operating and microstructure parameters on the cell performance. Consequently, in the present paper, the model was further validated for extended operating conditions (different fuel and oxidant compositions).

In addition, the present model is a continuum micro-scale model [3,4] which can, not only predict the detailed marco-scale cell performance, but also can predict the effects of microstructural electrode parameters, such as electrode thickness and porosity. Thus, this model serves as a bridge between micro-scale electrode models and macro-scale unit cell simulation, which is an important attribute of this model as a design tool. Model parameters such as cell structure parameters, chemical kinetics parameters, and transport properties were derived from experiments or published data. Note that for all simulation results presented here, all model parameters used are those that were determined in Ref. [1]; no additional tuning were performed in part II.

2. Model validation and discussion for extended operating conditions

2.1. Experimental and operating conditions

The test setup and characterization techniques were presented in part I of the present study [1]. In Ref. [1] only one binary mixture of H_2–H_2O was considered (4.2% H_2O from humidification at room temperature). This binary mixture is referred to in this paper as the base case (humidified H_2 with air at 1 atm for temperatures between 750 and 850 °C). In the present study, operating conditions and validation of the model are extended to various water contents and to ternary mixtures where H_2–H_2O is diluted with N_2. In addition, oxygen, instead of air, was also considered as oxidant. The flow rates of fuel and oxidant were kept at 50 sccm for all experiments. The polarization curves were measured using four-probe method. Each operating variables was varied as follows:

- cell temperatures: 750, 800 and 850 °C;
- oxidant: oxygen or air;
- water content in the fuel: the fuel gas was saturated at 30 °C (4.2% H_2O), 40 °C (7.3% H_2O) and 50 °C (12.4% H_2O);
- N_2 dilution: N_2 content in the dry fuel mixture: 0%, 20%, 40%, 60% and 80%

2.2. Effect of oxidant composition

The SOFC performance can be improved by using pure O_2 instead of air as oxidant. Fig. 1 depicts the modeling and experimental results at different temperatures when pure O_2 is used as oxidant. Note that the curves are shown for current densities

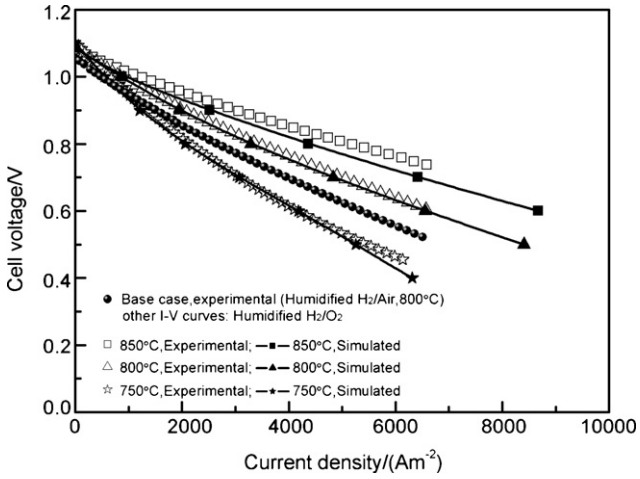

Fig. 1. Modeling and experimental polarization curves when using O_2 as oxidant at 750, 800 and 850 °C. Constant H_2O concentration of 4.2%.

up to 6500 A m^{-2} because 1 A is the maximum current allowed with the electrochemical workstation (IM6e, Zahner-Elektrik GmbH, Germany), which corresponds to a current density of around 6500 A m^{-2} for a cathode area of 1.54 cm^2.

It can be observed from Fig. 1 that the modeling results agree well with the experimental data at 750 and 800 °C, but somewhat underestimate the cell performance at 850 °C.

For comparison, the cell performance for the air case at 800 °C is also shown in Fig. 1. It is seen that the cell voltage at 800 °C is higher with pure O_2 than with air. At a current density of 6000 A m^{-2}, the difference in cell voltage is about 80 mV. Fig. 1 also shows that improvement in cell performance due to the use of pure oxygen increases as the current density increases.

2.3. Effects of fuel composition (mixtures of H_2/H_2O/N_2)

2.3.1. Effects of water content

Fig. 2 shows experimental and simulated cell performance data using air as oxidant when the fuel gas was humidified at 30, 40 and 50 °C, corresponding to a water content of 4.2%, 7.3% and 12.4%, respectively. Both experimental and simulated

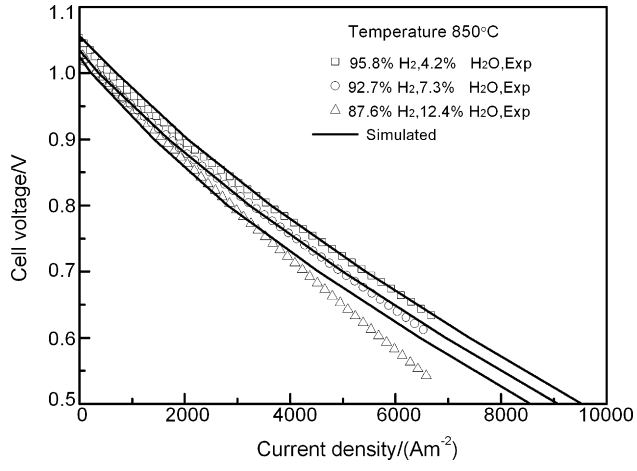

Fig. 2. Effects of water content on the cell performance.

polarization curves show that, as the water content increases, the cell performance deteriorates. The modeling results agree well with the experimental data when the fuel gas contains up to 7.3% water. For higher water content (e.g. 12.4%), the modeling results overestimate the cell performance, especially at higher current density. As discussed in Refs. [2,5], at higher current densities and higher product water concentrations, the competitive adsorption and surface diffusion mechanism may be responsible to higher interface diffusion resistance. However, the current model does not take into account the effects of competitive adsorption and surface diffusion, which might explain the difference between experimental and simulated results at higher water content and higher current densities.

2.3.2. *Effects of nitrogen content*

Fig. 3 shows the experimental and simulated polarization curves for various mixtures of $H_2/H_2O/N_2$ at 850 and 800 °C. In all cases, the water content was kept constant at 4.2%. Nitrogen does not contribute to the electrochemical reactions. However, not only N_2 could affect gas transport processes, but also, in the experiments shown in Fig. 3 the H_2O concentration was constant (constant humidification temperature) and therefore the H_2/H_2O ratio was changed as the N_2 concentration varied. It should be noted that experiments with large amounts of N_2 in the fuel are just carried out for model validation in this study, since such conditions will not be encountered in actual SOFC operation. Fig. 3 shows a reasonable agreement between experimental and simulated polarization curves at 850 °C, whereas at 800 °C the model results deviates from the experimental ones at high N_2 contents (above 50% N_2).

Both modeling and experimental results indicate that the open circuit voltage decrease as H_2 concentration decreases, which is more pronounced at 800 °C than at 850 °C. It is known that, for constant H_2/H_2O ratio, the open circuit voltage is not affected by the presence of inert gas [6]. The decrease in open circuit voltage seen in Fig. 3 is actually due to the change in H_2/H_2O ratio because the water content was kept constant at 4.2%. Comparison between the modeling results and experimental data in Fig. 3 indicates that the effects on cell performance by varying the H_2–N_2 composition becomes more significant at 800 °C than at 850 °C, especially at lower H_2 content. It is also clear that a limiting current density exists when N_2 content reaches 76.6% at 800 °C. At these conditions, although the simulated polarization curve deviates from the experimental one at high current densities, it is worth noticing that the simulated limiting current density (6470 A m^{-2}) matches well the limiting current density found experimentally (6430 A m^{-2}).

Fig. 3 highlights the effect of gas composition on cell performance. The gas composition affects essentially the open circuit voltage and anodic concentration overpotential. Fig. 4 shows the anodic concentration overpotential at two temperatures and two feed gas compositions. In this paper, the anodic concentration overpotential is not obtained from experiments. As a mathematical trick, if the source terms of the anode and cathode mass balance equations are set to zero, the fuel and oxidant concentrations are uniform throughout the electrodes and equal to the concentrations at the electrode/gas chamber interfaces. In this way, the effects of concentration overpotential could be separated. Since N_2 is inert with regard to charge transfer processes and has little effects on the adsorption equilibrium and surface diffusion processes [7], the important characteristic of the feed gas is the H_2/H_2O ratio. In Fig. 4 the two feed concentrations correspond to H_2/H_2O ratios of 18.2 (76.6% H_2) and 4.8 (19.2%). It can be seen from Fig. 4 that at 850 °C the

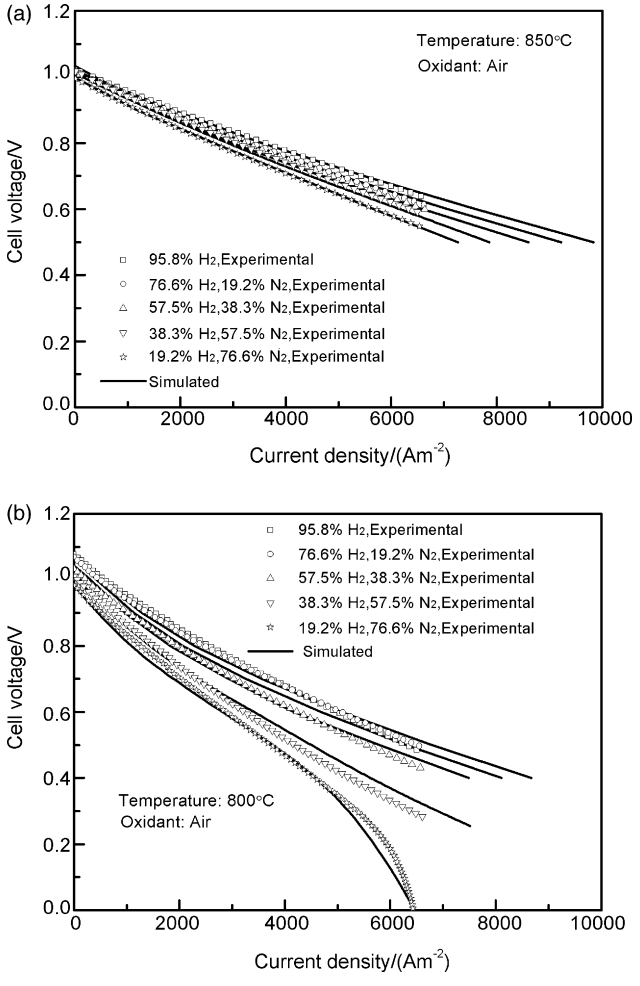

Fig. 3. Modeling and experimental polarization curves for various $H_2/H_2O/N_2$ fuel mixtures (a) 850 °C and (b) 800 °C. Constant H_2O concentration of 4.2%.

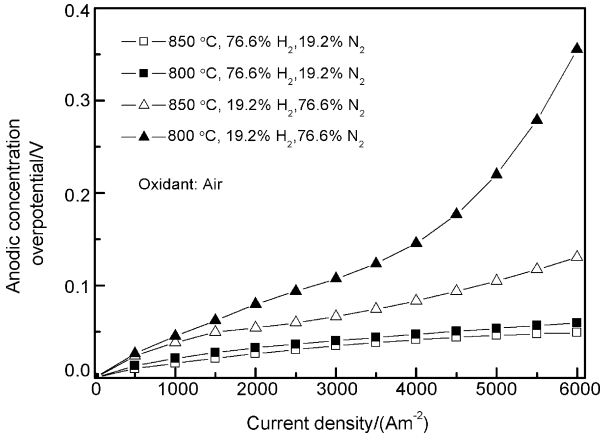

Fig. 4. Simulated anodic concentration overpotentials.

anodic concentration overpotential decreases only slightly as the H_2/H_2O ratio increases from 4.8 to 18.2. However, at 800 °C, the anodic concentration overpotential shows a dramatic increase when the H_2/H_2O ratio is decreased. This very large increase in anodic concentration overpotential is the reason for the rapid deterioration of the cell voltage observed in Fig. 3(b) at 800 °C and 19.2% H_2. At lower temperatures (e.g. 800 °C), the anodic concentration overpotential becomes more important due to a lower diffusion coefficient (diffusion through the porous anode) which is proportional to $T^{1.5}$. Also very important is the effect of multicomponent gas transport simulated here with the dusty gas model. The transport resistance increase when the H_2/H_2O ratio is decreased.

3. Simulation results and discussions

3.1. H_2 and H_2O concentration distributions

Fig. 5 shows the H_2 and H_2O concentrations at the anode for the case of H_2/H_2O 96%/4%, oxidant air, 800 °C and cell voltage 0.7 V. It can be seen that the concentration of H_2 decreases in the electrode from the fuel chamber/electrode interface to electrode/electrolyte interface, while the opposite is true for H_2O. This is due to the H_2 electrochemical oxidation at the reaction active sites resulting in the production of H_2O. The non-uniformity of H_2 and H_2O concentration distributions in Fig. 5 is due to the asymmetric electrode used in our button-cell. It can also be seen that the profiles of species mole fraction distribution vary faster near the electrolyte/anode active layer interface because of increased H_2 consumption and H_2O production rates.

3.2. Current density distribution

Fig. 6 gives the electronic current density distributions within the anode and cathode along the cell thickness direction ($r = 0$) for H_2/H_2O 96%/4%, oxidant air and 800 °C for various cell voltages. As expected, the cell voltage has a significant effect on the current density, which decreases as the cell voltage increases.

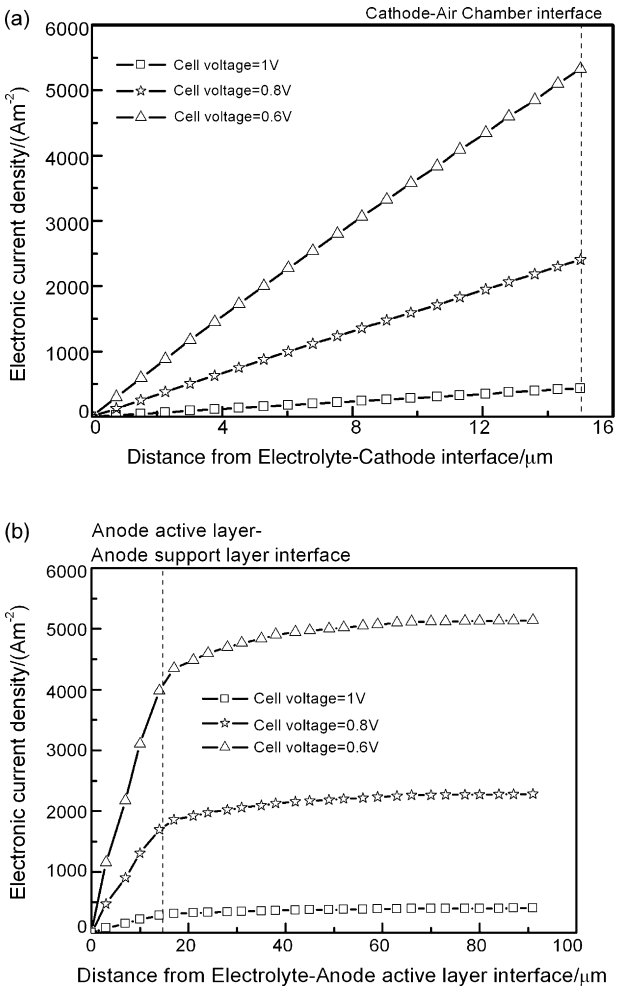

Fig. 6. Electronic current density distribution along the cell thickness direction ($r = 0$) in (a) cathode and (b) anode.

The electronic current density distribution can characterize the zone where the electrochemical reactions take place. Fig. 6(a) shows that the electrochemical reactions occurred within the whole cathode. It could then be deduced that the cell perfor-

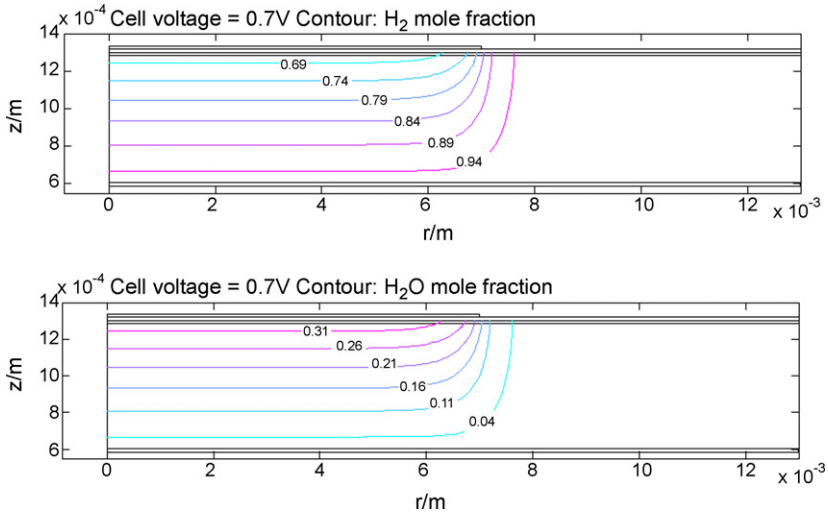

Fig. 5. Surface plots of H_2 and H_2O mole fractions.

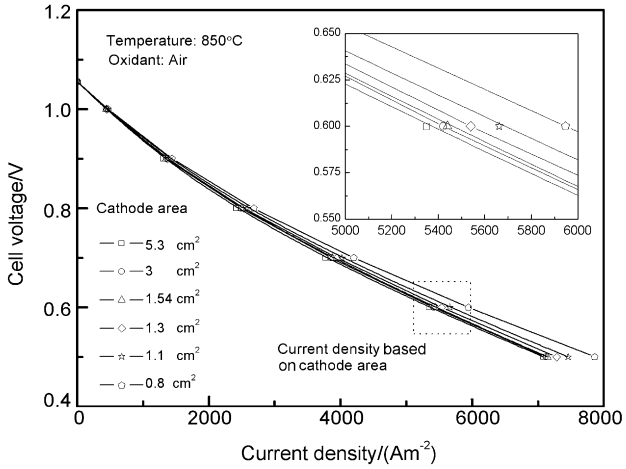

Fig. 7. Effects of cathode area on cell performance in the base case.

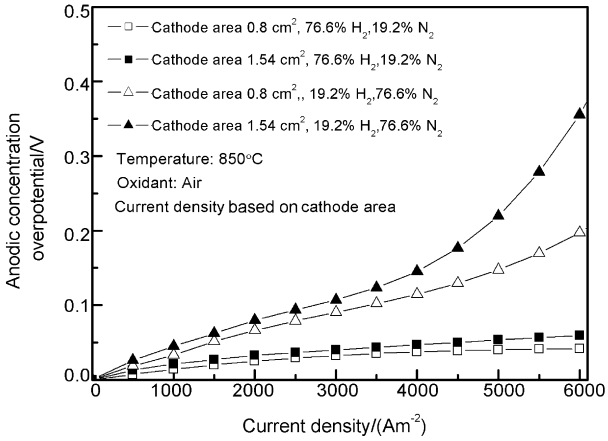

Fig. 8. Effects of cathode area on anodic concentration overpotential.

mance could be improved by adopting a cathode thicker than the 15 μm layer used in this study for a thicker cathode would supply more TPB active sites. Fig. 6(b) indicates that in the case of the anode most of the electrochemical reaction occurs mainly within a 20 μm distance from the electrolyte/anode active layer interface. It is also seen that the electrochemical reactions occur not only within the anode active layer, but also to some extent within the anode support layer. From the difference in curve slopes between the anode active and support layers, one can see that the electrochemical reaction rate at the anode active layer is larger than at the anode support layer. This is due to the difference in ionic conductivity and in reaction active area per unit volume. Thus, for this particular cell, it is likely that the cell performance can be improved by using a thicker anode active layer. However, since the mean pore size of the anode active layer is smaller than that of the anode support layer, increasing the active layer thickness will also increase diffusion resistance. Therefore, there should be an appropriate thickness for the active layer, which should not only depend on the active layer reactivity, but also on the layer microstructure. The effects of microstructure parameters and electrode thickness on cell performance are discussed in the next sections.

3.3. Effects of cathode area

Fig. 7 shows the simulated effects of cathode area on cell polarization curves for cells with cathode areas of 0.9, 1.1, 1.3, 1.54 (cathode area in button cell experiments), 3 and 5.3 cm^2 at 800 °C while keeping the anode area constant at 5.3 cm^2. The average current density was determined on the basis of the cathode area. It is seen (in the zoom window of Fig. 7) that the cell performance is slightly better when decreasing the cathode area, especially for the smallest area considered here. However, Fig. 7 also shows that the effects of cathode area is really small when the cathode area varies from 5.3 to 0.8 cm^2, which suggests that the effects of cathode area using an asymmetric electrode could almost be neglected in this case. However, the effect of cell performance due to asymmetric electrodes lies principally in the differences in anodic concentration polarization [5]. Fig. 8 shows the effects of cathode area on anodic concentration overpotential with different fuel compositions at 800 °C. This figure indicates that the anodic concentration overpotential increases only slightly as the cathode area increases from 0.8 to 1.54 cm^2 when the H_2 content in fuel mixtures is high (e.g. 76.6% H_2). However, when the H_2 content in fuel mixtures is low (e.g. 19.2% H_2) the effect of cathode area is more pronounced and could not be neglected. In this situation, the anodic concentration overpotential shows a rapid increase when the cathode area is increased, especially for current densities above 4000 A m^{-2}. This conclusion has also been experimentally supported in published data [8].

3.4. Effects of electrode porosity

An appropriate microstructure is a compromise between allowing sufficient paths for gas transport and keeping enough three-phase boundaries surface areas for the electrochemical reactions to take place. Porosity is one of the electrode microstructure parameters that usually affects the most the cell performance [4]. Usually, the ratio of porosity to tortuosity is used as a lumped parameter for representing the transport resistance. Thus, here the effects of porosity can represent the effects of this lumped parameter since the tortuosity was kept constant in the simulation.

Fig. 9 shows the effects of cathode and anode (both support and active layers) porosities on cell performance when operating at 0.7 V. Note that in this figure only one porosity is changed at a time. That is, the curve showing the effect of anode porosity, was determined a constant cathode porosity (36%) and vice versa for the effect of cathode porosity. The values of 36% for the porosity were determined from mercury porosimetry [1]. The temperature was set at 800 °C and all other parameters were the same as those in the base case. From Fig. 9, it is seen that the cell performance is slightly better when decreasing the cathode porosity or increasing the anode porosity. According to the calculation method to determine the TPB area per unit volume (S_{TPB}), increasing the porosity leads to a decrease in the S_{TPB}, but reduces mass transport resistance by increasing both the Knudsen and molecular effective diffusivities [9]. For instance, our

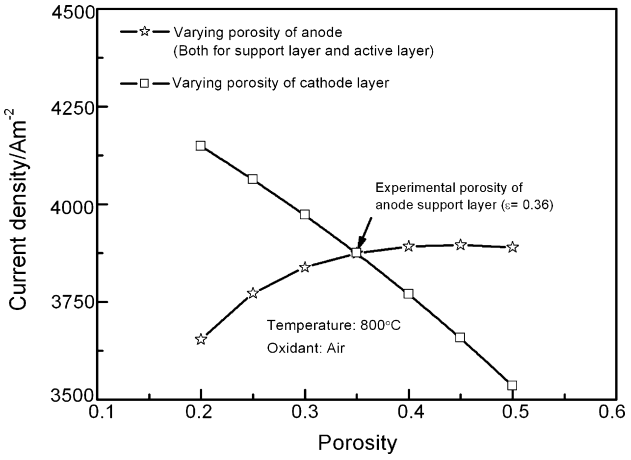

Fig. 9. Effects of electrode porosity on cell performance.

calculations have shown that when the porosity is varied from 0.2 to 0.5, the TPB area per unit volume of the electrode is reduced by a factor of 4, while the molecular diffusivity doubles and the Knudsen diffusivity increases about four times. Thus, for a thick electrode, as the anode in the present case, where concentration polarization may becomes limiting at a higher current density, increasing the porosity appropriately would improve the cell performance. On the other hand, for a thin electrode (e.g. cathode here) where concentration polarization is not a major issue, increasing porosity would make the cell performance worse.

3.5. Effects of mean particle size, mean pore size and electrode thickness

Fig. 10 shows the combined effects of mean particle size and electrode thickness when the cell voltage is kept at 0.7 V and the cell temperature kept at 800 °C. The changes in cell performance when varying the cathode thickness, anode active layer thickness and anode support layer thickness are shown in Fig. 10(a)–(c), respectively. Note that for each of these three figures, the layers whose thickness are not varied (e.g. anode active and support layers in Fig. 10(a)), are assumed to have a constant thickness equals to: 680 μm for the anode support layer, 15 μm for the anode active layer and cathode layer, and 20 μm for the thin-film electrolyte layer. In addition, the layers whose mean particle radius is not varied (e.g. particle radius of anode active and support layers in Fig. 10(a)) are assumed to have a constant value equals to: 0.6 μm for the anode support layer and cathode layer, 0.4 μm for the anode active layer. When the mean particle size of the electrode decreases, the TPB area per unit volume increases and the activation polarization is then expected to decrease. However, it should be noted that when the electrode mean particle radius decreases, the electrode mean pore radius also decreases, therefore increasing the concentration polarization because it becomes more difficult for the reactant gas to diffuse through the electrode due to the reduction of binary diffusion and Knudsen diffusion coefficients.

Fig. 10(a) shows the combined effects of the cathode mean particle size and thickness on cell performance. It is seen that the cell performance could be improved by adopting a thicker

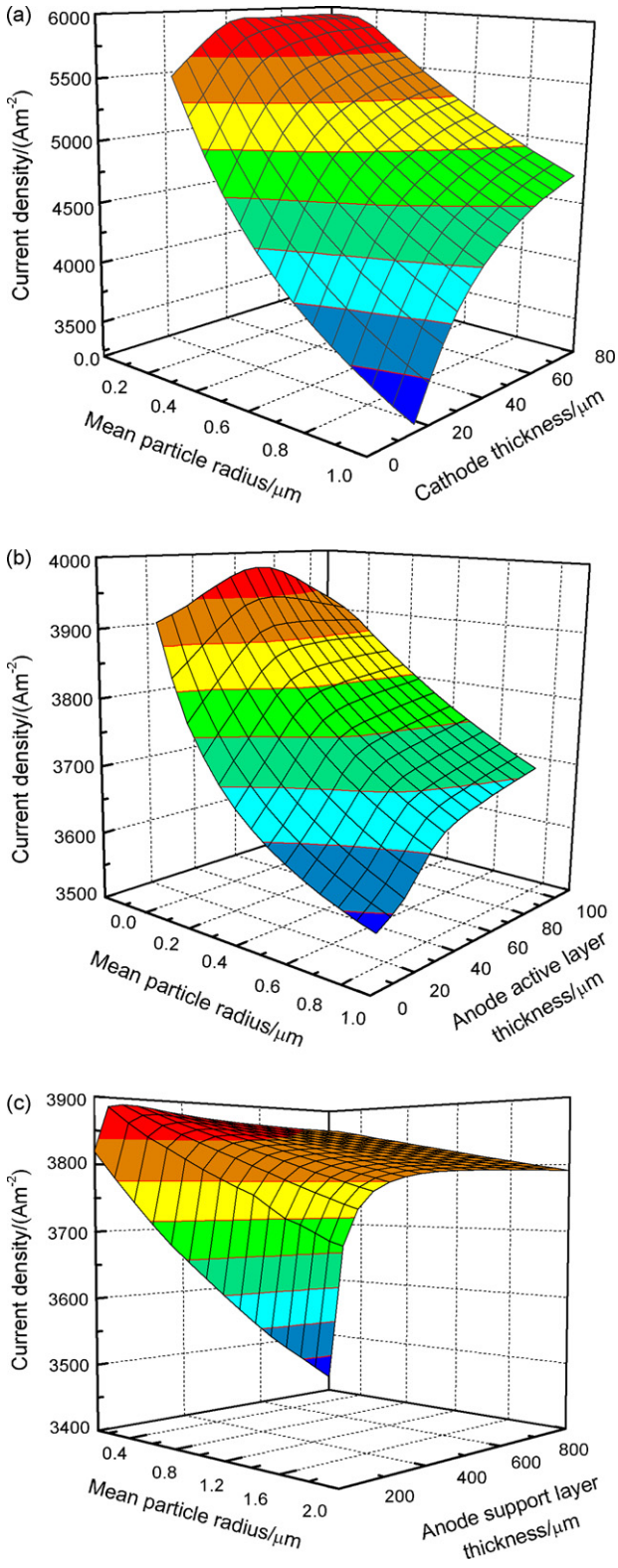

Fig. 10. Combined effects of mean particle size and layer thickness on the cell performance when changing the thickness of (a) cathode layer, (b) anode active layer and (c) anode support layer. All data for a temperature of 800 °C, cell voltage of 0.7 V and H_2/H_2O of 95.8%/4.2%.

cathode and a smaller mean particles radius, and this result was also supported by experimental data [10]. However, if the particle size is very small (e.g. <0.2 μm), increasing the cathode thickness will lead to an increase in cathodic concentration polarization. As a result there would be no benefit to increase the cathode thickness above around 30 μm. At a fixed cathode thickness, the cell performance is better with smaller mean particle size, because of the increase in TPB area per unit volume. From the previous discussion, the cell used in this work could be improved by increasing its cathode thickness and reducing its corresponding particle size.

Fig. 10(b) shows the combined effects of the anode active layer mean particle size and thickness on cell performance. It is seen from Fig. 10(b) that the cell performance can be optimized with smaller particle size and an appropriate active layer thickness. It should be noted that the effects of active layer thickness is much larger for mean particle radii larger than 0.6 μm. Also, as the mean particle size reduces, Fig. 10(b) shows that there is an appropriate active anode layer thickness yielding a maximum current density. For example, for a mean particle radius of 0.2 μm, the appropriate active anode layer thickness is around 60 μm. This highlights the opposite effects that the mean particle size can have on the concentration and activation overpotentials.

Fig. 10(c) shows that, as far as cell performance is concerned, an anode support layer thickness of 680 μm, as adopted in the base case, is not necessary. The cell performance would be very similar with a thickness of 300 μm. As for the cathode and the anode active layer, reducing the particle size has usually a beneficial effect on the cell performance. Yet, for very small particle sizes, concentration polarization may become dominant and an anode support layer too large would not be good. We should, however, keep in mind that the main function of the support anode layer is to ensure the mechanical strength of the PEN and thus its thickness should be kept at a relatively large value. To optimize the cell performance, the particle size of the anode support layer cannot be too small to prevent gas diffusion limitation.

The above discussion emphasized the importance of optimizing the cell microstructure parameters to achieve the highest performance. However, the electrode thickness and particle size are both limited by considerations such as manufacturing techniques or layer mechanical strength. The present modeling results should therefore, only be used as a basic guide for electrode design.

4. Conclusions

The two-dimensional isothermal mechanistic PEN model of an anode-supported solid oxide fuel cell for mixed gas, which was developed, calibrated and validated in part I of the present study, was further validated experimentally for extended operating conditions by changing temperatures, anode and cathode gas compositions. The validation results showed that the model agrees well with the experimental results for a wide range of operating conditions.

As expected both the modeling and experimental results show that the cell performance is better when operating at higher temperatures, using pure oxygen as oxidant and using a fuel with high hydrogen content.

Simulation of the electronic current density distribution gives an indication of the extent of the zone where the electrochemical reaction takes place. The results with our button cell suggest that the electrochemical reaction occurred within the whole cathode, the whole anode active layer, and also to some distance within anode support layer. Thus, it could be deduced that the cell performance could have been improved by adopting a thicker cathode or a thicker anode active layer. A sensitivity analysis on the anode and cathode porosities was then performed. This analysis indicated that for a thick electrode, as the anode in the present work, increasing the porosity would improve the cell performance, while for a thin electrode, as the cathode in current case, increasing porosity would have a negative effect on cell performance. The effects of electrode microstructure were further analyzed by investigating the combined effects of the thickness and particle size of each electrode layer (cathode, anode active layer and anode support layer). The modeling results indicated that the cell performance for our button cell could be optimized by adopting a thicker cathode with small particle size, a thicker anode active layer (but not too thick) with smaller particle size, and a thinner support layer. However, the electrode thickness and particle size are both limited by factors such as manufacturing technique or mechanical strength. Nonetheless, the model presented here can describe the effect of electrode microstructure on cell performance and can thus be a useful tool for electrode design.

References

[1] Y.X. Shi, N.S. Cai, C. Li, C. Bao, E. Croiset, J.Q. Qian, Q. Hu, S.R. Wang, Modeling of an anode-supported Ni-YSZ|Ni-ScSZ|ScSZ| LSM-ScSZ multiple layers SOFC cell. Part I. Experiments, model development and calibration. J. Power Sources, submitted for publication.
[2] Y.X. Shi, N.S. Cai, C. Li, J. Power Sources 164 (2007) 639–648.
[3] P. Costamagna, P. Costa, V. Antonucci, Electrochim. Acta 43 (1998) 375–394.
[4] S.H. Chan, Z.T. Xia, J. Electrochem. Soc. 148 (2001) A388–A394.
[5] R.E. Williford, L.A. Chick, G.D. Maupin, S.P. Simner, J.W. Stevenson, J. Electrochem. Soc. 150 (8) (2003) A1067–A1072.
[6] N.Q. Minh, T. Takahashi, Science and Technology of Ceramic Fuel Cells, Elsevier, Amsterdam, 1995, pp. 16–20.
[7] K. Sasaki, Y. Hori, R. Kikuchi, K. Eguchi, A. Ueno, H. Takeuchi, M. Aizawa, K. Tsujimoto, H. Tajiri, H. Nishikawa, Y. Uchida, J. Electrochem. Soc. 149 (2002) A227–A233.
[8] A.V. Virkar, Low-temperature, Anode-supported High Power Density Solid Oxide Fuel Cells with Nanostructured Electrodes, 2003 (contract no.: AC26-99FT40713).
[9] B. Todd, J.B. Young, J. Power Sources 110 (2002) 186–200.
[10] S.P. Jiang, P.J. Callus, S.P.S. Badwal, Solid State Ionics 132 (2000) 1–14.